Fast at-line characterization of solid organic waste: comparing analytical performance of different compact near infrared spectroscopic systems with different measurement configurations

Authors: Alexandre Mallet[a,b,c,d,], Margaud Périmé[a,d], Lorraine Awhangbo[a,d], Cyrille Charnier[c], Jean-Michel Roger[b,d], Jean-Philippe Steyer[a], Éric Latrille[a,d], Ryad Bendoula[b]*

[a)] INRAE, Univ Montpellier, LBE, 102 Av des Etangs, Narbonne F-11100, France

[b)] INRAE, UMR ITAP, Montpellier University, Montpellier, France

[c)] Bioentech, F-11100 Narbonne, France

[d)] ChemHouse Research Group, Montpellier, France

[*] **Corresponding author**
E-mail address: alexandre.mallet@bioentech.eu
Full postal address: INRAE-LBE, 102, Avenue des Etangs, F-11100 Narbonne

Abstract

Fast characterization of solid organic waste using near infrared spectroscopy has been successfully developed in the last decade. However, its adoption in biogas plants for monitoring the feeding substrates remains limited due to the lack of applicability and high costs. Recent evolutions in the technology have given rise to both more compact and more modular low-cost near infrared systems which could allow a larger scale deployment. The current study investigates the relevance of these new systems by evaluating four different Fourier transform near-infrared spectroscopic systems with different compactness (laboratory, portable, micro spectrometer) but also different measurement configurations (polarized light, at distance, in contact). Though the conventional laboratory spectrometer showed the best performance on the various biochemical parameters tested (carbohydrates, lipids, nitrogen, chemical oxygen demand, biochemical methane potential), the compact systems provided very close results. Prediction of the biochemical methane potential was possible using a low-cost micro spectrometer with an independent validation set error of only 91 $NmL(CH_4).gTS^{-1}$ compared to 60 $NmL(CH_4).gTS^{-1}$ for a laboratory spectrometer. The differences in performance were shown to result mainly from poorer spectral sampling; and not from instrument characteristics such as spectral resolution. Regarding the measurement configurations, none of the evaluated systems allowed a significant gain in robustness. In particular, the polarized light system provided better results when using its multi-

scattered signal which brings further evidence of the importance of physical light-scattering properties in the success of models built on solid organic waste.

Keywords

Near infrared spectroscopy; anaerobic digestion; process monitoring; biochemical methane potential; compact systems; measurement modes;

1. Introduction

In anaerobic digestion processes, different organic waste are often co-digested to enhance the production of both biogas and fertilizers (Hagos et al., 2017). A tremendous diversity of waste is concerned by these bioprocesses such as agricultural residues (animal manure, crop stems/stalks, silage), food industry waste (brewery, sugar refinery), urban solid waste, meat waste or catering waste. This implies that these waste cover a large range of biochemical composition and physical properties. Moreover, such properties may fluctuate according to factors such as crop seasonality, transport or storage. This brings important challenges for ensuring the stability of the process and the efficiency of biogas production in digesters (Wu et al., 2019). To answer this, online monitoring of the feeding substrate quality could allow the direct adaptation of the feeding strategy to the feeding substrate quality (Jacobi et al., 2011). However, up to today, this has only been shown

to be possible on digesters fed with a single type of substrate (like maize silage), while the usefulness of such system appears greater with important variations of substrate type and quality (Jacobi et al., 2012). In light of this, for co-digestion plants, there is a need for the development of fast and reliable characterization methods that are applicable on highly diverse organic waste.

Near infrared spectroscopy (NIRS), coupled with multivariate analysis techniques (Næs and Martens, 1984), has been successfully used as a fast and robust characterization method of solid organic waste (Skvaril et al., 2017). In the composting process, NIRS was used to monitor the degradation phases of compost (Albrecht et al., 2008), or to predict biochemical characteristics such as the carbon/nitrogen ratio (Vergnoux et al., 2009). In the anaerobic digestion process, the technology was initially used for in-situ monitoring of dry solids (DS), volatile solids (VS), chemical oxygen demand (COD) and volatile fatty acids (VFA) in digesters (Jacobi et al., 2009; Lomborg et al., 2009; Stockl and Lichti, 2018; Wolf et al., 2011). NIRS was then proposed for the determination of biochemical methane potential (BMP) on municipal solid waste (Lesteur et al., 2011), and has since been extended to other types of waste (Doublet et al., 2013; Fitamo et al., 2017; Godin et al., 2015; Triolo et al., 2014; Yang et al., 2021). Today, NIRS appears the most suitable method for predicting BMP on various organic substrates (Rodrigues et al., 2019). More recently, NIRS was used to estimate complementary characteristics such as carbohydrates content, lipid content, nitrogen content, COD, and kinetic parameters (Charnier et al., 2017). In terms of process monitoring, these developments

allow time-consuming reference measurements (which last typically one to two months for a characteristic like BMP) to be available in less than five days. Today, what limits the adoption of NIRS in full-scale biogas plants is its low applicability and high costs (Wu et al., 2019). Indeed, freeze-drying and grinding steps are necessary to avoid water and particle size effects in NIRS (Mallet et al., 2021), which currently limits the online applicability of such system. Moreover, the high costs of the spectrometer and the logistics involved in sending the sample at the laboratory still limits a regular and exhaustive analysis of the feeding substrates. Whether NIRS is applied directly on fresh waste or with a prior freeze-drying step, there is a need to develop cheap and reliable instruments which can be used on a wide range of substrate types in order to promote a greater adoption of NIRS in co-digestion plants. This could be addressed by an at-site use of low-cost and compact near infrared (NIR) systems.

In the past few years, the use of NIRS has developed out of laboratories, thanks to important progress in the miniaturization of instruments. In particular, handheld Fourier transform near infrared (FT-NIR) micro spectrometers have appeared in the market, and make use of a micro-electro-mechanical systems-based (MEMS) Michelson interferometer (Beć et al., 2021). While conventional Michelson interferometers are made of discrete elements (including the moving mirror actioned by a motor, the fixed mirror, and beam splitter), MEMS technology enables a monolithic integration of these elements on a single chip, with the particularity that the moving mirror is operated by an electrical signal. Amongst the spectrometers

making use of this technology, the NeoSpectra instrument has shown good analytical performance results for soil organic and total carbon content characterization (Sharififar et al., 2019; Tang et al., 2020), or authenticity screening in food (McVey et al., 2021). These compact spectrometers allow the measurements to be performed on site, thanks to their compactness, robustness and cost. However, these compact portable spectrometers tend to have poorer instrument performances than laboratory spectrometer, with lower resolution, spectral range, and signal-to-noise ratio (Beć et al., 2020; Crocombe, 2018). Therefore, the suitability of such systems for the characterization of diverse organic waste still needs to be assessed.

Another aspect of these compact systems concerns their modularity and the possibility of testing different measurement configurations, in order to enhance the measured signal. Indeed, in complex matter such as solid organic waste, the Bouguer-Beer-Lambert law does not hold due to important light scattering (Dahm and Dahm, 2004). To answer this, spectral pre-processing has been proposed to remove both additive and multiplicative effects (Rabatel et al., 2020; Rinnan et al., 2009; Zeaiter et al., 2005) and thus, make the problem linear again. However, other developments have rather focused on enhancing the measured signal directly. A promising optical pre-processing method, based on polarized light spectroscopy (Backman et al., 1999) has been proposed to improve the absorbance signal measurement on such scattering samples (Bendoula et al., 2015; Gobrecht et al., 2015; Xu et al., 2019). Such system has shown analytical performance improvements for soils (Gobrecht et al., 2016), and more recently, for digestate (Awhangbo

et al., 2020), but has never been evaluated on solid organic waste. Still in the aim of enhancing the measured spectra, time-resolved spectroscopy shows a promising future : applied to pharmaceutical tablets, collected photons with a particular propagation time were shown to be most informative for quantification (Alayed and Deen, 2017; Johansson et al., 2002). However, the cost of this technology still remains prohibitive for the organic waste management sector. Finally, the measurement mode (at distance or in contact, in reflectance or in interactance) also plays an important role in the final accuracy for estimating biochemical properties (Hemrattrakun et al., 2021; Khodabakhshian et al., 2019; Schaare and Fraser, 2000). Though current used laboratory spectrometers make use of a distance reflectance measurement, a contact immerged probe measurement has been shown to be useful for prediction of parameters on digestates (Awhangbo et al., 2020). Authors observe higher reflectance levels with less noise in the collected spectra, as well as new chemical features which were not apparent in a remote probe configuration. In light of this, it appears that the use of different measurement configurations could enable the calibration of more accurate and more robust NIRS models on diverse solid organic waste.

As mentioned, the applicability of compact and low-cost spectroscopic systems remains to be assessed for biochemical characterization of highly diverse solid organic waste. Moreover, the modularity offered by such compact systems is a unique opportunity to evaluate whether the use of different measurement configurations can help build more robust models. This study aims to assess these two

matters by comparing the analytical performances of four different NIRS systems: a standard laboratory spectrometer, a portable spectrometer with two measurement configurations (contact mode and polarized mode), and a micro-spectrometer. For this purpose, measurements were acquired with each system on a selection of solid organic waste. Then, for each spectroscopic system, prediction models for five biochemical characteristics (carbohydrates, lipids, nitrogen, COD and BMP) were calibrated and their performances were compared.

2. Materials and Methods

2.1. Sample preparation and reference analyses

Thirty-three substrates were selected amongst various waste types that have been collected in rural, territorial and industrial anaerobic digestion plants in France. These substrates cover a wide range of biochemical and physical properties: solid cellulosic waste (like silage, cereals and corn cobs), liquid cellulosic suspensions (such as manure), liquid fat suspensions (catering waste or biowaste), sweet emulsions (such as lactoserum), or protein and fat solid pastes (such as egg waste or cacao butter). The visual aspect of some of these substrates in raw form is presented in Appendix A.

For spectral measurements, each substrate sample was freeze-dried and ground to 1 mm. The dataset is fully described in a data paper [On-site substrate characterization in the anaerobic digestion context: a dataset of NIR spectra acquired with

four different optical systems on freeze-dried and ground organic waste – this data paper is submitted jointly with this article, reference will need an update after reviewing] and available online [https://doi.org/10.15454/SQQTUU].

Biochemical characterization of substrates was obtained by using a NIRS calibrated model (Charnier et al., 2017), with errors on independent test sets of 53 $mg(O_2).gTS^{-1}$ for carbohydrates content, $3.2*10^{-2}$ $g.gTS^{-1}$ for lipids content, 8.6 $mg.gTS^{-1}$ for nitrogen content, and 83 $mg(O_2).gTS^{-1}$ for COD. The histograms of obtained prediction values are presented in Figure 1.

2.2. Spectroscopic systems

The four spectroscopic systems compared in this study are presented below. In addition, spectral measurement protocols are compared in Table 1.

2.2.1. Laboratory spectroscopic system

The laboratory spectroscopic system consists of a NIR-Flex N-500 solids FT-NIR spectrophotometer with a vial accessory (Buchi, Flawil, Switzerland), scanning in reflectance mode with a spectral range of 4 000 cm^{-1} to 10 000 cm^{-1} (1000-2500 nm) and a resolution of 4 cm^{-1}. An external white reference (Spectralon®) signal $I_0(\lambda)$ is automatically taken every 10 minutes. For each sample, an intensity signal $I(\lambda)$ was collected, and the pseudo-absorbance signal $A_{lab}(\lambda)$ was computed:

$$A_{lab}(\lambda) = -log_{10}\left(R_{lab}(\lambda)\right) = -log_{10}\left(\frac{I(\lambda)}{I_0(\lambda)}\right). \quad \text{(Eq. 1)}$$

187

188 2.2.2. Portable spectrometer with immersed contact probe

189 The immersed contact probe system consists of a FT-NIR Rocket spectrometer
190 (Arcoptix, Neuchatel, Switzerland) scanning in reflectance mode with a spectral
191 range of 3 800 cm^{-1} to 11 000 cm^{-1} (900-2500 nm) and a resolution of 4 cm^{-1}. The
192 spectrometer was connected to two optical fibers (for illumination and signal collec-
193 tion) of 1000 µm core diameter and numerical aperture of 0.39 (BFY1000,
194 Thorlabs). A tungsten-halogen source (Ocean Optics HL-200-FHSA) was used for
195 illumination. For each sample, the intensity $I(\lambda)$ was collected. A white reference
196 (SRS99, Spectralon®) was scanned every hour during the measurements resulting
197 in $I_0(\lambda)$. Finally, a dark current signal $I_n(\lambda)$ corresponding to the instrumental noise
198 was recorded and subtracted to all spectra. A pseudo-absorbance signal $A_{ip}(\lambda)$
199 was thus calculated:
200

$$A_{ip}(\lambda) = -log_{10}\left(R_{ip}(\lambda)\right) = -log_{10}\left(\frac{I(\lambda) - I_n(\lambda)}{I_0(\lambda) - I_n(\lambda)}\right). \quad \text{(Eq. 2)}$$

201

202 2.2.3. Portable spectrometer with polarized light spectroscopy

203

204 The polarized light system consists of the same elements (spectrometer, light
205 source, optical fibers) as the immersed contact probe system, however, measure-

206 ments were made at a distance of 5 cm from the samples, and a polarized light
207 component (Awhangbo et al., 2020) was connected to the spectrometer. This
208 component consisted in a wire-grid polarizer (Thorlabs WP25L-UB) to s-polarize
209 the incident light; and a calcite Wolaston polarizer (Thorlabs WP10P) to split the
210 reflected light in an s-polarized and p-polarized image, corresponding to parallel
211 $I_{\parallel}(\lambda)$ and perpendicular $I_{\perp}(\lambda)$ light signals. As in the previous system, both the dark
212 current signal $I_n(\lambda)$, and a white reference signal $I_0(\lambda) = I_{\parallel}(\lambda)_0 + I_{\perp}(\lambda)_0$ were col-
213 lected. Three signals were then calculated following Bendoula et al. (2015) formula
214 (Bendoula et al., 2015): the single scattering reflectance $R_{ss}(\lambda)$, the multiple scat-
215 tering reflectance $R_{ms}(\lambda)$, and the total backscattering reflectance $R_{bs}(\lambda)$:

$$R_{ss}(\lambda) = \frac{(I_{\parallel}(\lambda) - I_n(\lambda)) - (I_{\perp}(\lambda) - I_n(\lambda))}{I_0(\lambda) - I_n(\lambda)}. \quad \text{(Eq. 3)}$$

$$R_{ms}(\lambda) = \frac{2(I_{\perp}(\lambda) - I_n(\lambda))}{I_0(\lambda) - I_n(\lambda)}. \quad \text{(Eq. 4)}$$

$$R_{bs}(\lambda) = \frac{(I_{\parallel}(\lambda) - I_n(\lambda)) + (I_{\perp}(\lambda) - I_n(\lambda))}{I_0(\lambda) - I_n(\lambda)}. \quad \text{(Eq. 5)}$$

216

217 ### 2.2.4. Handheld micro spectrometer

218 The micro spectrometer system consists of a MEMS FT-NIR NeoSpectra spec-
219 trometer (Si-Ware, Cairo, Egypt) scanning in reflectance mode with a spectral
220 range of 3 921 cm^{-1} to 7 407 cm^{-1} (1350-2550 nm) and a resolution of 66 cm^{-1}. A
221 white reference (SRS99, Spectralon®) signal $I_0(\lambda)$ was collected before each

measurement. For each sample, an intensity signal $I(\lambda)$ was collected and the pseudo-absorbance signal $A_\mu(\lambda)$ was computed:

$$A_\mu(\lambda) = -log_{10}\left(R_\mu(\lambda)\right) = -log_{10}\left(\frac{I(\lambda)}{I_0(\lambda)}\right). \quad \text{(Eq. 6)}$$

2.3. Data analysis: model calibration

All the data analysis was performed using Python 3.6.5: data wrangling with Pandas 0.25.1, NumPy 1.17.3, SciPy 1.3.1, Scikit-learn 0.21.3, and plotting with Matplotlib 2.2.2 (Harris et al., 2020; Hunter, 2007; McKinney, 2010; Pedregosa et al., 2015; van Rossum and Drake, 2009; Virtanen et al., 2020).

Measurements of the 33 substrates on the four spectroscopic configurations yielded six different matrices : the absorbance signal A_{lab} from the laboratory spectrometer, the absorbance signal A_{ip} from the immerged contact probe system, the three reflectance signals R_{ss}, R_{ms} and R_{bs} (respectively single scattered, multiple scattered, total back-scattered) from the polarized system, and finally the absorbance signal A_μ from the micro spectrometer system.

For noise reduction and baseline correction, a selection of seven pretreatments that have proven to be efficient in previous studies on organic waste (Charnier et al., 2017; Lesteur et al., 2011) have been used: the standard normal variate (Barnes et al., 1989) (SNV), the first-order detrend (Barnes et al., 1989) (DT1), the first-order Savitzky-Golay (Savitzky and Golay, 1964) derivation (SG1), the sec-

241 ond-order Savitzky-Golay derivation (SG2), combinations of SNV and first-order
242 Savitzky-Golay derivation (SNV+SG1 or SG1+SNV) and finally, a weighted EMSC
243 with variable sorting for normalization (VSN) (Rabatel et al., 2020). The raw signal
244 was used directly as well, which resulted overall in testing eight different prepro-
245 cessing conditions.
246 In order to evaluate the models built on each spectroscopic system, a validation
247 test set was constituted. With the aim of producing a representative validation test
248 set, the Duplex algorithm (Snee, 1977) was run for each reference characteristic
249 (carbohydrates content, lipid content, total nitrogen content, COD, BMP). This re-
250 sulted in a training set of 22 substrates, and a validation test set of 11 substrates.
251 To assess the representativeness of the validation test set in terms of spectral var-
252 iability, a principal components analysis (Cordella, 2012) was done, and obtained
253 scores were plot in Figure 2 and Appendix C.
254 Models were built using a partial least squares regression (PLS1-R) with NI-
255 PALS algorithm (Næs and Martens, 1984; WOLD, 1973). To determine the number
256 of latent variables, a cross-validation was done using a repeated randomized
257 group-k-fold cross-validation with $k = 5$ the fold number and $n\_repeats = 30$ the
258 repetition number. Sample triplicates were always kept within one fold to ensure
259 independence. For each cross-validation run, various metrics were then calculated:
260 the root-mean-square error (RMSE), the mean absolute error (MAE) (Willmott and
261 Matsuura, 2005), the coefficient of determination (R^2), and B-coefficients metrics
262 which are the Durbin-Watson statistic (DW) and the variance (Rutledge and
263 Barros, 2002). The choice of the number of latent variables was made by analyzing

all these metrics together (i.e. choosing the minimal number of latent variables while minimizing RMSE and MAE, maximizing R^2, and detecting rate increase of DW and variance of B-coefficients).

Spectral range was also optimized for each of the signal types. This was done by calibrating a first model, analyzing its B-coefficients (available in Appendix E), and shrinking the spectral range adequately before recalibrating the model.

The final performances of the obtained models were evaluated on the validation test set, based on the root-mean-square error (RMSE) and the coefficient of determination (R^2).

To assess prediction repeatability of a given model, the variance of each sample's triplicate spectra predictions was calculated:

$$s_r^2 = \sum_{i=1}^{3} (\hat{y}_i - \bar{\hat{y}})^2, \qquad \text{(Eq. 7)}$$

and the global prediction repeatability standard deviation was calculated as the quadratic mean of each s_r:

$$S_r = \sqrt{\sum_{i=1}^{n\_test\_samples} {s_r^2}_i}. \qquad \text{(Eq. 8)}$$

3. Results & Discussion

3.1. Data overview

3.1.1. Training set and validation test set

For each reference characteristic, train and test set distributions (respectively in blue and orange) are presented as histograms in Figure 1. Very similar distributions (same mean, same standard deviation) for all characteristics show that the Duplex algorithm succeeded in obtaining a representative test set in terms of biochemical composition. To complete this analysis, the representativeness in terms of signal is assessed by looking at the scores of train and test sets for each signal type in Figure 2 (only the first and second component scores are displayed, but scores up to the tenth component were checked). As shown, the test set signals (in orange) cover most of the range covered by train set signals. However, in some cases, the variability of train set signals is not fully well represented in the test set. For example, in the upper left score plot representing the laboratory spectrometer configuration signal A_{lab}, no test set signal (orange square) is found in the far right plot where there are two train set signals (blue triangles). This is consistent with the fact that the Duplex algorithm was run on the reference values and not on the spectral values, so there is no guarantee for test set spectral representativeness. Although this is not optimal for evaluating calibration models alone, such method-

300 ology appeared to be the best to compare different spectroscopic systems on iden-
301 tical samples without bias.
302

303 ### 3.1.2. Raw spectra analysis

304

305 Figure 3 presents the raw reflectance signals obtained with each spectroscopic
306 system. In all signals, the main peaks found in organic waste were apparent: the
307 CH, CH_2 and CH_3 combination bands particularly present in fat (1731 nm, 1764
308 nm, 2310 nm, 2350 nm), the OH bands present in simple sugars (1436 nm, 1932
309 nm), the OH combination bands in starch or cellulose (2092 nm), and the NH com-
310 bination bands present in proteins (2180 nm) (Williams and Antoniszyn, 2019;
311 Workman Jr. and Weyer, 2012). However, the relative amplitude of these peaks
312 seems to differ. For example, in the micro spectrometer signal (R_μ) the CH_2 combi-
313 nation bands at 2310 nm and 2350 nm seem much less sharp than in the laborato-
314 ry spectrometer signal (R_{lab}). This can be well explained by the lower resolution of
315 the micro-spectrometer (66 cm^{-1}) compared to the laboratory spectrometer (4 cm^{-1}).
316 A consequence of this is that the models built on compact systems such as the
317 micro spectrometer will be based on more simple features, which could lead them
318 to be less accurate models but potentially also more robust.
319 In addition, the sensitivity with respect to the spectral range appears to differ from
320 one spectrometer to another. For the micro spectrometer, the measured signal be-
321 low 1600 nm seems much noisier than in other systems. Such sharp peaks are

not, *a priori*, expected in NIR spectra of complex matter. Similarly, for the immersed probe contact (R_{ip}) or polarized signals (R_{ss}, R_{ms}, R_{bs}), it seems the measured signals below 1200 nm and over 2240 nm are as well very noisy. For this reason, these spectral regions were later removed from the calibration of the built models.

Another point of comparison concerns the observed reflectance levels (Figure 4). The reflectance levels of R_{lab}, R_{bs}, and R_{μ} are much higher (with 75% of the values that range respectively between 0.46 and 0.73, 0.43 and 0.66, and 0.60 and 0.90), than the reflectance levels of R_{ip} (with 75% of the values that range between 0.15 and 0.35). This is mostly related to the way the signal is acquired (i.e. the measurement configuration). Indeed, reflectance levels are the result of both the absorption level (dependent of chemical composition) and the scattering level (modifications of light optical path-length, and photon leakage (Gobrecht et al., 2014)). Therefore, the chosen measurement configuration might favour one or the other, leading to differences in the measured reflectance levels. Results show here that the distant mode systems (i.e. R_{lab}, R_{bs}, and R_{μ}) collect much more scattering photons than the contact mode system (i.e. R_{ip}). Regarding the advantage of one measurement mode over the other, this will mostly be dependent on the characteristic to be predicted, and its dependency on physical properties.

In the polarized light system, a clear difference of reflectance level can also be observed: 75% of the values of the multiple scattering signal R_{ms} range between 0.52 and 0.76, against 0.05 and 0.11 for the single scattering signal R_{ss}. This is con-

sistent with the sole principle of polarized spectroscopy where R_{ss} corresponds to single scattering photons with low penetration in the media while R_{ms} corresponds to multiple scattering photons with a longer optical path length in the media due to refraction events. This further confirms the efficiency of polarized spectroscopy as an optical method to remove the scattering effects in the measured signal (Bendoula et al., 2015; Gobrecht et al., 2016). However, the impacts on the subsequent models built on such signals remain to be studied.

3.2. Model performances

For the five reference characteristics that were studied, the best selected models obtained on each of the six signals are presented in Table 2.

For prediction models built using the laboratory spectrometer system, the errors obtained on the test set (RMSEP) were of 0.108 $g.gTS^{-1}$ for carbohydrates content, 5.8 $mg.gTS^{-1}$ for nitrogen content, 0.034 $g.gTS^{-1}$ for lipids content, 0.060 $NL(CH_4).gTS^{-1}$ for BMP, and 136.4 $mg(O_2).gTS^{-1}$ for COD. These are all consistent to the performances of reference models (Charnier et al., 2017). The slightly lower performances obtained can be explained by the more limited number of samples on which these models were built (22 samples) compared to the original models (about 80 samples).

For all predicted characteristics, the laboratory system (A_{lab}) showed better analytical performance results than the compact systems (A_{ip}, A_{μ}, R_{ss}, R_{ms}, R_{bs}). However, in many cases, these latter systems showed similar performances to the labora-

365 tory system. For example, for BMP prediction, the prediction error (RMSEP) of the
366 model obtained with the laboratory spectrometer signal A_{lab} was 60 mL(CH_4).gTS^{-1}.
367 In comparison, for the polarized system signals R_{ss}, R_{ms}, R_{bs}, the model prediction
368 errors were of respectively 115 mL(CH_4).gTS^{-1}, 111 mL(CH_4).gTS^{-1} and 100
369 mL(CH_4).gTS^{-1} , while for the micro spectrometer signal A_{μ} the model's error was of
370 only 91 mL(CH_4).gTS^{-1}. Similarly, for carbohydrates content prediction, while the
371 prediction error for the laboratory spectrometer was 0.108 g.gTS^{-1}, the errors for
372 the micro-spectrometer and the immersed probe system were of only 0.134 g.gTS^{-1}
373 and 0.104 g.gTS^{-1}. Such observation can be made for all the other characteristics
374 studied. This is very promising because these models have acceptable errors
375 compared to the laboratory spectrometer. This means that the models built on or-
376 ganic waste rely on sufficiently simple features so that the lower spectral resolution
377 of compact spectrometers does not affect too much the performances. Such result
378 is consistent with similar studies on low-cost compact NIR spectrometers with lim-
379 ited spectral range that are applied to herbaceous feedstock such as corn stover or
380 sorghum (Wolfrum et al., 2020). Knowing that these spectrometers are low-cost
381 (while the laboratory spectrometer costs about 50 000€, the immersed contact
382 probe and polarized systems each cost about 20 000€ and the micro spectrometer
383 only costs about 3 000 €), and can be used at-site, this holds great promises re-
384 garding an increased adoption of NIRS for robust solid organic waste characteriza-
385 tion in anaerobic digestion plants.
386

387 Models built on the three signals R_{ss}, R_{ms}, R_{bs} obtained using the polarized spec-
388 troscopy system show different performances. While R_{bs} is a signal very similar to
389 those obtained from the other set-ups because it includes information from all the
390 backscattering light, R_{ss} and R_{ms} differ in terms of type of photons that are captured
391 by the spectrometer (respectively single scattering photons, and multiple scattering
392 photons). For all characteristics, models built on R_{bs} signal show better perfor-
393 mances than models built on the R_{ss} and R_{ms} signals. For example, for COD pre-
394 diction, while the prediction error (RMSEP) of the model using the total back-
395 scattering signal (R_{bs}) is of 129.2 mg(O_2).gTS^{-1}, it is of 147.8 mg(O_2).gTS^{-1} using
396 R_{ms} and 273.9 mg(O_2).gTS^{-1} using R_{ss}. This suggests that the use of polarized
397 spectroscopy for predicting these characteristics on organic waste may not be par-
398 ticularly recommended.
399 In fact, for lipids content, COD and nitrogen content, the models built with R_{ss} sig-
400 nals show much greater errors than models built with R_{ms} signals (respectively
401 0.124 g.gTS^{-1} greater than 0.068 g.gTS^{-1}, 273.9 mg(O_2).gTS^{-1} greater than 147.8
402 mg(O_2).gTS^{-1}, and 21.4 mg.gTS^{-1} greater than 12.1 mg.gTS^{-1}). This came as a
403 surprise, as the single scattering signal is theoretically supposed to be more relat-
404 ed to absorbing constituents and less impacted by scattering effects (Gobrecht et
405 al., 2015). This can be explained by the fact that for a dataset with such diverse
406 solid organic substrates, the biochemical composition is closely related to the phys-
407 ical properties. For example, high lipid content substrates (which also correspond
408 to substrates with high COD) tend to form liquid transparent solutions (like oil),
409 which transmit light much more than low lipid content substrates which usually form

410 highly scattering porous media. This relatively poor performance obtained with the
411 single scattering signal is consistent with results obtained on digestates where
412 physical structure appeared determinant (Awhangbo et al., 2020). One additional
413 reason can be found in the measurement technique itself: the intensity captured for
414 the single scattering signal is much more limited than a classical total backscatter-
415 ing signal, leading to higher signal-to-noise ratios. Further investigations could
416 concentrate on the use of a multi-block approach combining these three comple-
417 mentary signals, as proposed on digestates (Awhangbo et al., 2020).
418
419 Apart from the single scattering signal, all signals allowed to build satisfactory
420 models for the biochemical characterization of organic waste. However, no spec-
421 troscopic system allowed to surpass the analytical performance of the laboratory
422 spectrometer system. Figure 5 presents the observed and prediction plots for each
423 signal for the prediction of biochemical potential. In A_{lab} (upper left subplot), the
424 predictions for each of the three replicate spectra do not differ (for one observed
425 value, the prediction values are overlaid on the graph); while for the other spectro-
426 scopic systems, the predictions for each of the three replicate spectra are very dif-
427 ferent. For example, the sample with a BMP of 0.63 $NL(CH_4)g.TS^{-1}$ has predictions
428 that vary for A_{lab} between 0.869 $NL(CH_4)g.TS^{-1}$ and 0.870 $NL(CH_4)g.TS^{-1}$, while the
429 predictions for A_{ip} and A_{μ} vary respectively between 0.863 $NL(CH_4)g.TS^{-1}$ and
430 0.940 $NL(CH_4)g.TS^{-1}$ and between 0.709 $NL(CH_4)g.TS^{-1}$ and 0.771 $NL(CH_4)g.TS^{-1}$.
431 This is observed for all the other characteristics as shown in Appendix D. It ap-
432 pears that in all the compact systems, the replicate spectra vary much more from

433 each other than with the laboratory spectrometer. This could explain the greater
434 errors obtained using the compact systems. The following result may be investi-
435 gated more quantitatively by calculating the global repeatability standard deviations
436 as presented in Figure 6. Indeed, for all characteristics, the compact systems show
437 much higher repeatability standard deviations than the laboratory spectrometer (in
438 red). Such differences are due to the way the spectral measurements are acquired.
439 As detailed in Table 1, the systems do not have the same number of scans and
440 sampling surface. While for one measurement, the laboratory spectrometer collects
441 scans during a full rotation of the sampling cup, the other systems only collect
442 scans on a fixed point of the sample's surface. This means that in
443 compact systems the spectral measurement is much less representative of the to-
444 tal sample. It appears that the performance of compact systems could be en-
445 hanced by optimizing the way the spectra are taken: increasing the number of
446 scans and the number of replicates to ensure a better stability of the measure-
447 ments.
448
449 While the suitability of the compact and low-cost spectrometers has been demon-
450 strated, some challenges remain. Though models could be calibrated on the com-
451 pact systems' signals directly as in this study, it is most probable that models will
452 remain being built and maintained on standard laboratory spectrometers, with
453 transfer functions being built between the laboratory spectrometer (referred as the
454 "master" spectrometer) and the compact spectrometers (referred as the "slave"
455 spectrometers). This transfer approach has already been proven to be successful

between a laboratory spectrometer and an online spectrometer for in situ monitoring of anaerobic digestion (Krapf et al., 2013). However, the robustness of these transfer functions applied to compact systems still needs to be assessed.

4. Conclusions

Results have shown that compact and low-cost systems including a hand-held micro spectrometer are suitable for online characterization of diverse solid organic waste. However, the use of new measurement configurations such as the polarized mode was not shown to be an effective way to enhance the quality of predictive models. This suggests that the physical scattering properties of the substrates are the main determinant of analytical performance of NIRS calibration models built on such highly diverse solid organic waste. Keys for the improvement of the compact systems appear to lie in further optimization of the sampling protocol. These results set the path to a new era of low-cost and on-site NIRS analysis of the feeding substrates in co-digestion plants.

Acknowledgements

Financial support from the National Research Institute for Agriculture, Food and Environment (INRAE), the French Agency of National Research and Technology (ANRT) [grant number 2018/0461] and the Biogaz-RIO platform [FEDER-FSE Languedoc Roussillon 2014-2020] is hereby acknowledged.

References

Alayed, M., Deen, M.J., 2017. Time-resolved diffuse optical spectroscopy and imaging using solid-state detectors: Characteristics, present status, and research challenges. Sensors (Switzerland) 17, 2115. https://doi.org/10.3390/s17092115

Albrecht, R., Joffre, R., Gros, R., Le Petit, J., Terrom, G., Périssol, C., 2008. Efficiency of near-infrared reflectance spectroscopy to assess and predict the stage of transformation of organic matter in the composting process. Bioresour. Technol. 99, 448–455. https://doi.org/10.1016/j.biortech.2006.12.019

Awhangbo, L., Bendoula, R., Roger, J.M., Béline, F., 2020. Multi-block SO-PLS approach based on infrared spectroscopy for anaerobic digestion process monitoring. Chemom. Intell. Lab. Syst. 196, 103905. https://doi.org/10.1016/j.chemolab.2019.103905

Backman, V., Gurjar, R., Badizadegan, K., Itzkan, I., Dasari, R.R., Perelman, L.T., Feld, M.S., 1999. Polarized light scattering spectroscopy for quantitative measurement of epithelial cellular structures in situ. IEEE J. Sel. Top. Quantum Electron. 5, 1019–1026. https://doi.org/10.1109/2944.796325

Barnes, R.J., Dhanoa, M.S., Lister, S.J., 1989. Standard normal variate transformation and de-trending of near-infrared diffuse reflectance spectra. Appl. Spectrosc. 43, 772–777. https://doi.org/10.1366/0003702894202201

Beć, K.B., Grabska, J., Huck, C.W., 2021. Principles and Applications of Miniaturized Near-Infrared (NIR) Spectrometers. Chem. - A Eur. J. 27, 1514–1532. https://doi.org/10.1002/chem.202002838

Beć, K.B., Grabska, J., Siesler, H.W., Huck, C.W., 2020. Handheld near-infrared spectrometers: Where are we heading? NIR news 31, 28–35. https://doi.org/10.1177/0960336020916815

499 Bendoula, R., Gobrecht, A., Moulin, B., Roger, J.M., Bellon-Maurel, V., 2015. Improvement
500 of the chemical content prediction of a model powder system by reducing multiple
501 scattering using polarized light spectroscopy. Appl. Spectrosc. 69, 95–102.
502 https://doi.org/10.1366/14-07539
503 Charnier, C., Latrille, E., Jimenez, J., Lemoine, M., Boulet, J.C., Miroux, J., Steyer, J.P.,
504 2017. Fast characterization of solid organic waste content with near infrared
505 spectroscopy in anaerobic digestion. Waste Manag. 59, 140–148.
506 https://doi.org/10.1016/j.wasman.2016.10.029
507 Cordella, C.B.Y., 2012. PCA: The Basic Building Block of Chemometrics, in: Krull, I.S.
508 (Ed.), Analytical Chemistry. IntechOpen, pp. 1–46. https://doi.org/10.5772/51429
509 Crocombe, R.A., 2018. Portable Spectroscopy. Appl. Spectrosc. 72, 1701–1751.
510 https://doi.org/10.1177/0003702818809719
511 Dahm, K.D., Dahm, D.J., 2004. Relation of representative layer theory to other theories of
512 diffuse reflection. J. Near Infrared Spectrosc. 12, 189–198.
513 https://doi.org/10.1255/jnirs.426
514 Doublet, J., Boulanger, A., Ponthieux, A., Laroche, C., Poitrenaud, M., Cacho Rivero, J.A.,
515 2013. Predicting the biochemical methane potential of wide range of organic
516 substrates by near infrared spectroscopy. Bioresour. Technol. 128, 252–258.
517 https://doi.org/10.1016/j.biortech.2012.10.044
518 Fitamo, T., Triolo, J.M., Boldrin, A., Scheutz, C., 2017. Rapid biochemical methane
519 potential prediction of urban organic waste with near-infrared reflectance
520 spectroscopy. Water Res. 119, 242–251. https://doi.org/10.1016/j.watres.2017.04.051
521 Gobrecht, A., Bendoula, R., Roger, J.M., Bellon-Maurel, V., 2016. A new optical method
522 coupling light polarization and Vis-NIR spectroscopy to improve the measurement of
523 soil carbon content. Soil Tillage Res. 155, 461–470.

https://doi.org/10.1016/j.still.2015.06.003

Gobrecht, A., Bendoula, R., Roger, J.M., Bellon-Maurel, V., 2015. Combining linear polarization spectroscopy and the Representative Layer Theory to measure the Beer-Lambert law absorbance of highly scattering materials. Anal. Chim. Acta 853, 486–494. https://doi.org/10.1016/j.aca.2014.10.014

Gobrecht, A., Roger, J.M., Bellon-Maurel, V., 2014. Major Issues of Diffuse Reflectance NIR Spectroscopy in the Specific Context of Soil Carbon Content Estimation. A Review., Advances in Agronomy. https://doi.org/10.1016/B978-0-12-420225-2.00004-2

Godin, B., Mayer, F., Agneessens, R., Gerin, P., Dardenne, P., Delfosse, P., Delcarte, J., 2015. Biochemical methane potential prediction of plant biomasses: Comparing chemical composition versus near infrared methods and linear versus non-linear models. Bioresour. Technol. 175, 382–390. https://doi.org/10.1016/j.biortech.2014.10.115

Hagos, K., Zong, J., Li, D., Liu, C., Lu, X., 2017. Anaerobic co-digestion process for biogas production: Progress, challenges and perspectives. Renew. Sustain. Energy Rev. 76, 1485–1496. https://doi.org/10.1016/j.rser.2016.11.184

Harris, C.R., Millman, K.J., van der Walt, S.J., Gommers, R., Virtanen, P., Cournapeau, D., Wieser, E., Taylor, J., Berg, S., Smith, N.J., Kern, R., Picus, M., Hoyer, S., van Kerkwijk, M.H., Brett, M., Haldane, A., del Río, J.F., Wiebe, M., Peterson, P., Gérard-Marchant, P., Sheppard, K., Reddy, T., Weckesser, W., Abbasi, H., Gohlke, C., Oliphant, T.E., 2020. Array programming with NumPy. Nature 585, 357–362. https://doi.org/10.1038/s41586-020-2649-2

Hemrattrakun, P., Nakano, K., Boonyakiat, D., Ohashi, S., Maniwara, P., Theanjumpol, P., Seehanam, P., 2021. Comparison of Reflectance and Interactance Modes of Visible

549 and Near-Infrared Spectroscopy for Predicting Persimmon Fruit Quality. Food Anal.
550 Methods 14, 117–126. https://doi.org/10.1007/s12161-020-01853-w
551 Hunter, J.D., 2007. Matplotlib: A 2D graphics environment. Comput. Sci. Eng. 9, 90–95.
552 https://doi.org/10.1109/MCSE.2007.55
553 Jacobi, H.F., Moschner, C.R., Hartung, E., 2011. Use of near infrared spectroscopy in
554 online-monitoring of feeding substrate quality in anaerobic digestion. Bioresour.
555 Technol. 102, 4688–4696. https://doi.org/10.1016/j.biortech.2011.01.035
556 Jacobi, H.F., Moschner, C.R., Hartung, E., 2009. Use of near infrared spectroscopy in
557 monitoring of volatile fatty acids in anaerobic digestion. Water Sci. Technol. 60, 339–
558 346. https://doi.org/10.2166/wst.2009.345
559 Jacobi, H.F., Ohl, S., Thiessen, E., Hartung, E., 2012. NIRS-aided monitoring and
560 prediction of biogas yields from maize silage at a full-scale biogas plant applying
561 lumped kinetics. Bioresour. Technol. 103, 162–172.
562 https://doi.org/10.1016/j.biortech.2011.10.012
563 Johansson, J., Folestad, S., Josefson, M., Sparen, A., Abrahamsson, C., Andersson-
564 Engels, S., Svanberg, S., 2002. Time-resolved NIR/vis spectroscopy for analysis of
565 solids: Pharmaceutical tablets. Appl. Spectrosc. 56, 725–731.
566 https://doi.org/10.1366/000370202760077676
567 Khodabakhshian, R., Emadi, B., Khojastehpour, M., Golzarian, M.R., 2019. A comparative
568 study of reflectance and transmittance modes of Vis/NIR spectroscopy used in
569 determining internal quality attributes in pomegranate fruits. J. Food Meas. Charact.
570 13, 3130–3139. https://doi.org/10.1007/s11694-019-00235-z
571 Krapf, L.C., Nast, D., Gronauer, A., Schmidhalter, U., Heuwinkel, H., 2013. Transfer of a
572 near infrared spectroscopy laboratory application to an online process analyser for in
573 situ monitoring of anaerobic digestion. Bioresour. Technol. 129, 39–50.

https://doi.org/10.1016/j.biortech.2012.11.027

Lesteur, M., Latrille, E., Maurel, V.B., Roger, J.M., Gonzalez, C., Junqua, G., Steyer, J.P., 2011. First step towards a fast analytical method for the determination of Biochemical Methane Potential of solid wastes by near infrared spectroscopy. Bioresour. Technol. 102, 2280–2288. https://doi.org/10.1016/j.biortech.2010.10.044

Lomborg, C.J., Holm-Nielsen, J.B., Oleskowicz-Popiel, P., Esbensen, K.H., 2009. Near infrared and acoustic chemometrics monitoring of volatile fatty acids and dry matter during co-digestion of manure and maize silage. Bioresour. Technol. 100, 1711–1719. https://doi.org/10.1016/j.biortech.2008.09.043

Mallet, A., Charnier, C., Latrille, É., Bendoula, R., Steyer, J.-P., Roger, J.-M., 2021. Unveiling non-linear water effects in near infrared spectroscopy: A study on organic wastes during drying using chemometrics. Waste Manag. 122, 36–48. https://doi.org/10.1016/j.wasman.2020.12.019

McKinney, W., 2010. Data Structures for Statistical Computing in Python, in: Proceedings of the 9th Python in Science Conference. pp. 56–61. https://doi.org/10.25080/majora-92bf1922-00a

McVey, C., McGrath, T.F., Haughey, S.A., Elliott, C.T., 2021. A rapid food chain approach for authenticity screening: The development, validation and transferability of a chemometric model using two handheld near infrared spectroscopy (NIRS) devices. Talanta 222, 121533. https://doi.org/10.1016/j.talanta.2020.121533

Næs, T., Martens, H., 1984. Multivariate calibration. II. Chemometric methods. Trends Anal. Chem. 3, 266–271. https://doi.org/10.1016/0165-9936(84)80044-8

Pedregosa, F., Varoquaux, G., Buitinck, L., Louppe, G., Grisel, O., Mueller, A., 2015. Scikit-learn: Machine Learning in Python. J. Mach. Learn. Res. 19, 29–33.

Rabatel, G., Marini, F., Walczak, B., Roger, J.M., 2020. VSN: Variable sorting for

normalization. J. Chemom. 34, 1–16. https://doi.org/10.1002/cem.3164

Rinnan, Å., Berg, F. van den, Engelsen, S.B., 2009. Review of the most common pre-processing techniques for near-infrared spectra. TrAC - Trends Anal. Chem. 28, 1201–1222. https://doi.org/10.1016/j.trac.2009.07.007

Rodrigues, R.P., Rodrigues, D.P., Klepacz-Smolka, A., Martins, R.C., Quina, M.J., 2019. Comparative analysis of methods and models for predicting biochemical methane potential of various organic substrates. Sci. Total Environ. 649, 1599–1608. https://doi.org/10.1016/j.scitotenv.2018.08.270

Rutledge, D.N., Barros, A.S., 2002. Durbin-Watson statistic as a morphological estimator of information content. Anal. Chim. Acta 454, 277–295. https://doi.org/10.1016/S0003-2670(01)01555-0

Savitzky, A., Golay, M.J.E., 1964. Smoothing and Differentiation of Data by Simplified Least Squares Procedures. Anal. Chem. 36, 1627–1639. https://doi.org/10.1021/ac60214a047

Schaare, P.N., Fraser, D.G., 2000. Comparison of reflectance, interactance and transmission modes of visible-near infrared spectroscopy for measuring internal properties of kiwifruit (Actinidia chinensis). Postharvest Biol. Technol. 20, 175–184. https://doi.org/10.1016/S0925-5214(00)00130-7

Sharififar, A., Singh, K., Jones, E., Ginting, F.I., Minasny, B., 2019. Evaluating a low-cost portable NIR spectrometer for the prediction of soil organic and total carbon using different calibration models. Soil Use Manag. 35, 607–616. https://doi.org/10.1111/sum.12537

Skvaril, J., Kyprianidis, K.G., Dahlquist, E., 2017. Applications of near-infrared spectroscopy (NIRS) in biomass energy conversion processes: A review. Appl. Spectrosc. Rev. 52, 675–728. https://doi.org/10.1080/05704928.2017.1289471

624 Snee, R.D., 1977. Validation of Regression Models: Methods and Examples.
625 Technometrics 19, 415–428. https://doi.org/10.1080/00401706.1977.10489581
626 Stockl, A., Lichti, F., 2018. Near-infrared spectroscopy (NIRS) for a real time monitoring of
627 the biogas process. Bioresour. Technol. 247, 1249–1252.
628 https://doi.org/10.1016/j.biortech.2017.09.173
629 Tang, Y., Jones, E., Minasny, B., 2020. Evaluating low-cost portable near infrared sensors
630 for rapid analysis of soils from South Eastern Australia. Geoderma Reg. 20, e00240.
631 https://doi.org/10.1016/j.geodrs.2019.e00240
632 Triolo, J.M., Ward, A.J., Pedersen, L., Løkke, M.M., Qu, H., Sommer, S.G., 2014. Near
633 Infrared Reflectance Spectroscopy (NIRS) for rapid determination of biochemical
634 methane potential of plant biomass. Appl. Energy 116, 52–57.
635 https://doi.org/10.1016/j.apenergy.2013.11.006
636 van Rossum, G., Drake, F.L., 2009. Python 3 Reference Manual, CreateSpace. Scotts
637 Valley, CA. https://doi.org/10.5555/1593511
638 Vergnoux, A., Guiliano, M., Le Dréau, Y., Kister, J., Dupuy, N., Doumenq, P., 2009.
639 Monitoring of the evolution of an industrial compost and prediction of some compost
640 properties by NIR spectroscopy. Sci. Total Environ. 407, 2390–2403.
641 https://doi.org/10.1016/j.scitotenv.2008.12.033
642 Virtanen, P., Gommers, R., Oliphant, T.E., Haberland, M., Reddy, T., Cournapeau, D.,
643 Burovski, E., Peterson, P., Weckesser, W., Bright, J., van der Walt, S.J., Brett, M.,
644 Wilson, J., Millman, K.J., Mayorov, N., Nelson, A.R.J., Jones, E., Kern, R., Larson, E.,
645 Carey, C.J., Polat, İ., Feng, Y., Moore, E.W., VanderPlas, J., Laxalde, D., Perktold, J.,
646 Cimrman, R., Henriksen, I., Quintero, E.A., Harris, C.R., Archibald, A.M., Ribeiro,
647 A.H., Pedregosa, F., van Mulbregt, P., Vijaykumar, A., Bardelli, A. Pietro, Rothberg,
648 A., Hilboll, A., Kloeckner, A., Scopatz, A., Lee, A., Rokem, A., Woods, C.N., Fulton,

C., Masson, C., Häggström, C., Fitzgerald, C., Nicholson, D.A., Hagen, D.R., Pasechnik, D. V., Olivetti, E., Martin, E., Wieser, E., Silva, F., Lenders, F., Wilhelm, F., Young, G., Price, G.A., Ingold, G.L., Allen, G.E., Lee, G.R., Audren, H., Probst, I., Dietrich, J.P., Silterra, J., Webber, J.T., Slavič, J., Nothman, J., Buchner, J., Kulick, J., Schönberger, J.L., de Miranda Cardoso, J.V., Reimer, J., Harrington, J., Rodríguez, J.L.C., Nunez-Iglesias, J., Kuczynski, J., Tritz, K., Thoma, M., Newville, M., Kümmerer, M., Bolingbroke, M., Tartre, M., Pak, M., Smith, N.J., Nowaczyk, N., Shebanov, N., Pavlyk, O., Brodtkorb, P.A., Lee, P., McGibbon, R.T., Feldbauer, R., Lewis, S., Tygier, S., Sievert, S., Vigna, S., Peterson, S., More, S., Pudlik, T., Oshima, T., Pingel, T.J., Robitaille, T.P., Spura, T., Jones, T.R., Cera, T., Leslie, T., Zito, T., Krauss, T., Upadhyay, U., Halchenko, Y.O., Vázquez-Baeza, Y., 2020. SciPy 1.0: fundamental algorithms for scientific computing in Python. Nat. Methods 17, 261–272. https://doi.org/10.1038/s41592-019-0686-2

Williams, P., Antoniszyn, J., 2019. Near-infrared Technology: Getting the best out of light. African Sun Media. https://doi.org/10.18820/9781928480310

Willmott, C.J., Matsuura, K., 2005. Advantages of the mean absolute error (MAE) over the root mean square error (RMSE) in assessing average model performance. Clim. Res. 30, 79–82. https://doi.org/10.3354/cr030079

WOLD, H., 1973. Nonlinear Iterative Partial Least Squares (NIPALS) Modelling: Some Current Developments, Multivariate Analysis–III. Academic press, Inc. https://doi.org/10.1016/b978-0-12-426653-7.50032-6

Wolf, D., von Canstein, H., Schröder, C., 2011. Optimisation of biogas production by infrared spectroscopy-based process control. J. Nat. Gas Sci. Eng. 3, 625–632. https://doi.org/10.1016/j.jngse.2011.07.006

Wolfrum, E.J., Payne, C., Schwartz, A., Jacobs, J., Kressin, R.W., 2020. A Performance

674 Comparison of Low-Cost Near-Infrared (NIR) Spectrometers to a Conventional
675 Laboratory Spectrometer for Rapid Biomass Compositional Analysis. Bioenergy Res.
676 https://doi.org/10.1007/s12155-020-10135-6
677 Workman Jr., J., Weyer, L., 2012. Practical Guide and Spectral Atlas for Interpretive Near-
678 Infrared Spectroscopy. CRC press. https://doi.org/10.1201/b11894
679 Wu, D., Li, L., Zhao, X., Peng, Y., Yang, P., Peng, X., 2019. Anaerobic digestion: A review
680 on process monitoring. Renew. Sustain. Energy Rev. 103, 1–12.
681 https://doi.org/10.1016/j.rser.2018.12.039
682 Xu, J.L., Gobrecht, A., Gorretta, N., Héran, D., Gowen, A.A., Bendoula, R., 2019.
683 Development of a polarized hyperspectral imaging system for investigation of
684 absorption and scattering properties. J. Near Infrared Spectrosc. 27, 314–329.
685 https://doi.org/10.1177/0967033519857732
686 Yang, G., Li, Y., Zhen, F., Xu, Y., Liu, J., Li, N., Sun, Y., Luo, L., Wang, M., Zhang, L.,
687 2021. Biochemical methane potential prediction for mixed feedstocks of straw and
688 manure in anaerobic co-digestion. Bioresour. Technol. 326, 124745.
689 https://doi.org/10.1016/j.biortech.2021.124745
690 Zeaiter, M., Roger, J.M., Bellon-Maurel, V., 2005. Robustness of models developed by
691 multivariate calibration. Part II: The influence of pre-processing methods. TrAC -
692 Trends Anal. Chem. 24, 437–445. https://doi.org/10.1016/j.trac.2004.11.023

693

Tables

Table 1. Spectral measurement protocol characteristics.

	Laboratory spectrometer	**Immersed contact probe**	**Polarization system**	**Micro spectrometer**
Measurement replicates	3	3	3	3
Number of scans per measurement	96 scans	10 scans	10 scans	28s scan time
Measurement sampling method (measured area per scan)	360° rotation (~5 cm^2)	Fixed point (~0.05 cm^2)	Fixed point (~1 cm^2)	Fixed point (~25 cm^2)
Protocol between replicates	Mix the whole sample	Change the measured surface position	Change the measured surface position	Change the measured surface position

Table 2. Descriptive statistics of the calibrated models. For each predicted reference measurement (carbohydrates, nitrogen, lipids, BMP, COD), the retained model for each spectroscopic system signal (A_{lab}, A_{ip}, A_{μ}, R_{ss}, R_{ms}, R_{bs}) is presented. The optimized parameters are provided (the spectral range, the pretreatment and the number of latent variables) along with the different performance metrics (RMSEC, RMSECV, RMSEP, R^2C, R^2P).

Experiment	Optimized parameters				Performance metrics				
Reference	**Signal**	**Spectral range (nm)**	**Pretreatment**	**#LV**	**$RMSE_C$**	**$RMSE_{CV}$**	**$RMSE_P$**	**R^2_C**	**R^2_P**
Carbohydrates	**A_{lab}**	1400-2240	SNV+SG1	2	0.143	0.192	0.108	0.78	0.83
g.gTS^{-1}	**A_{ip}**	1450-2240	SNV	2	0.188	0.169	0.104	0.82	0.84
	A_u	1400-2500	SNV+SG1	3	0.146	0.137	0.134	0.75	0.88
	R_{ss}	1200-2240	SNV	2	0.259	0.296	0.207	0.28	0.37
	R_{ms}	1200-2240	Raw	4	0.121	0.185	0.112	0.82	0.82
	R_{bs}	1300-2300	SNV+SG1	3	0.119	0.158	0.130	0.74	0.91
Nitrogen	**A_{lab}**	1200-2240	SNV+SG1	10	3.6	15.0	5.8	0.98	0.89
mg.gTS^{-1}	**A_{ip}**	1200-2240	SNV+SG1	5	9.9	18.4	7.5	0.87	0.83
	A_u	1400-2500	SNV	5	10.1	20.7	13.1	0.85	0.51
	R_{ss}	1200-2240	SG2	3	17.2	23.1	21.4	0.62	-0.4
	R_{ms}	1200-2240	SNV+SG1	5	12.6	22.6	12.1	0.80	0.54
	R_{bs}	1300-2300	SG1+SNV	4	10.7	17.6	11.7	0.83	0.61
Lipids	**A_{lab}**	1400-2240	SNV	6	0.025	0.056	0.034	0.99	0.98
g.gTS^{-1}	**A_{ip}**	1200-2240	VSN	9	0.057	0.066	0.066	0.99	0.93
	A_u	1400-2500	SG1+SNV	6	0.039	0.081	0.067	0.98	0.92
	R_{ss}	1200-2240	Raw	5	0.084	0.110	0.124	0.91	0.74
	R_{ms}	1200-2240	SG2	5	0.029	0.059	0.068	0.99	0.92

	R_{bs}	1200-2480	SG2	6	0.029	0.066	0.066	0.99	0.93
BMP	A_{lab}	1400-2240	SNV+SG1	9	0.020	0.078	0.060	0.99	0.90
NL(CH_4).gTS^{-1}	A_{ip}	1200-2240	SG1	2	0.088	0.115	0.110	0.77	0.73
	A_u	1600-2500	SG2	2	0.102	0.109	0.091	0.74	0.82
	R_{ss}	1200-2240	SG1	4	0.085	0.115	0.115	0.79	0.71
	R_{ms}	1350-2240	SG1	3	0.087	0.115	0.111	0.78	0.73
	R_{bs}	1300-2300	SG1	6	0.046	0.120	0.100	0.94	0.78
COD	A_{lab}	1400-2240	SNV	6	63.0	186.8	136.4	0.97	0.94
mg(O_2).gTS^{-1}	A_{ip}	1450-2240	SNV+SG1	7	106.2	228.3	160.2	0.93	0.90
	A_u	1400-2500	SG1+SNV	3	180.4	303.1	196.9	0.81	0.85
	R_{ss}	1200-2240	SG2	4	192.0	247.4	273.9	0.78	0.72
	R_{ms}	1350-2240	SG1	3	112.5	151.4	147.8	0.92	0.92
	R_{bs}	1200-2480	SG1+SNV	4	128.1	237.6	129.2	0.90	0.94

704

Figures

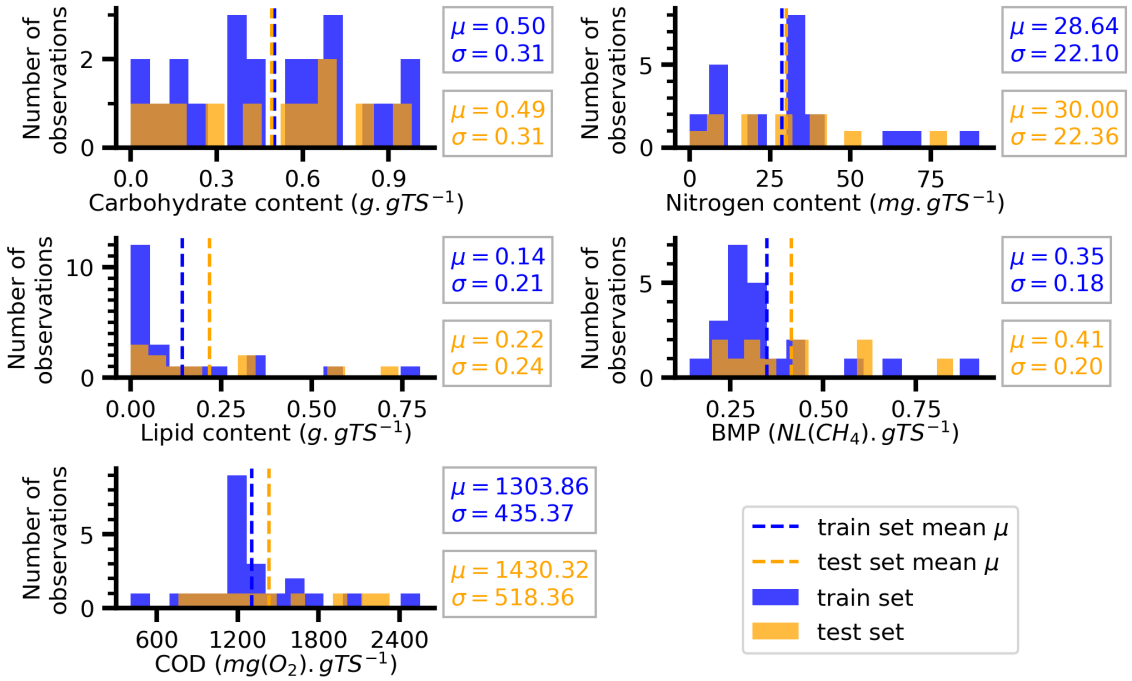

Figure 1. Histograms of reference characteristics. Both train and test sets (respectively in blue and in orange) obtained by a Duplex split are presented. Respective mean (labeled as μ) and standard deviation (labeled as σ) are presented for train and test sets (respectively in blue, and in orange). Dotted lines represent respective mean values.

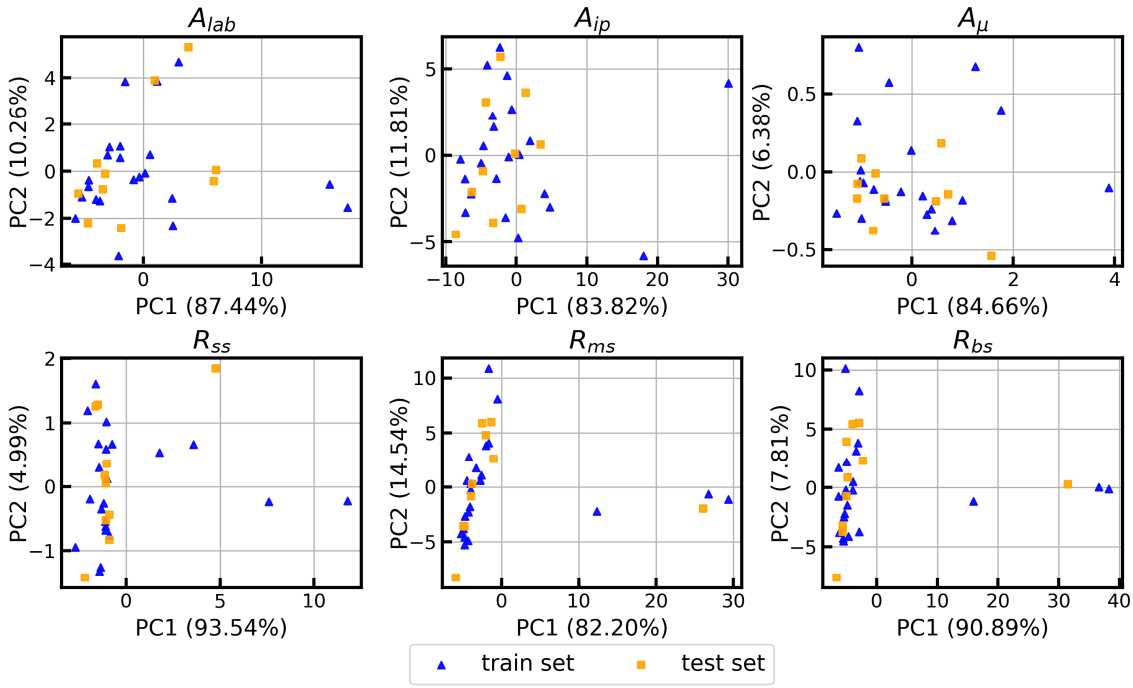

Figure 2. Principal component analysis (PCA) score plots of train and test sets (respectively in blue triangles, and in orange squares) for each signal type (from the four spectroscopic configurations). Each subplot represents the scores of the first and second principal components (PC1 and PC2). The percentage of explained variance is provided in the labels. The train and test split was obtained by a Duplex split based on the carbohydrates content levels. Score plots for other reference characteristics are shown in Appendix C.

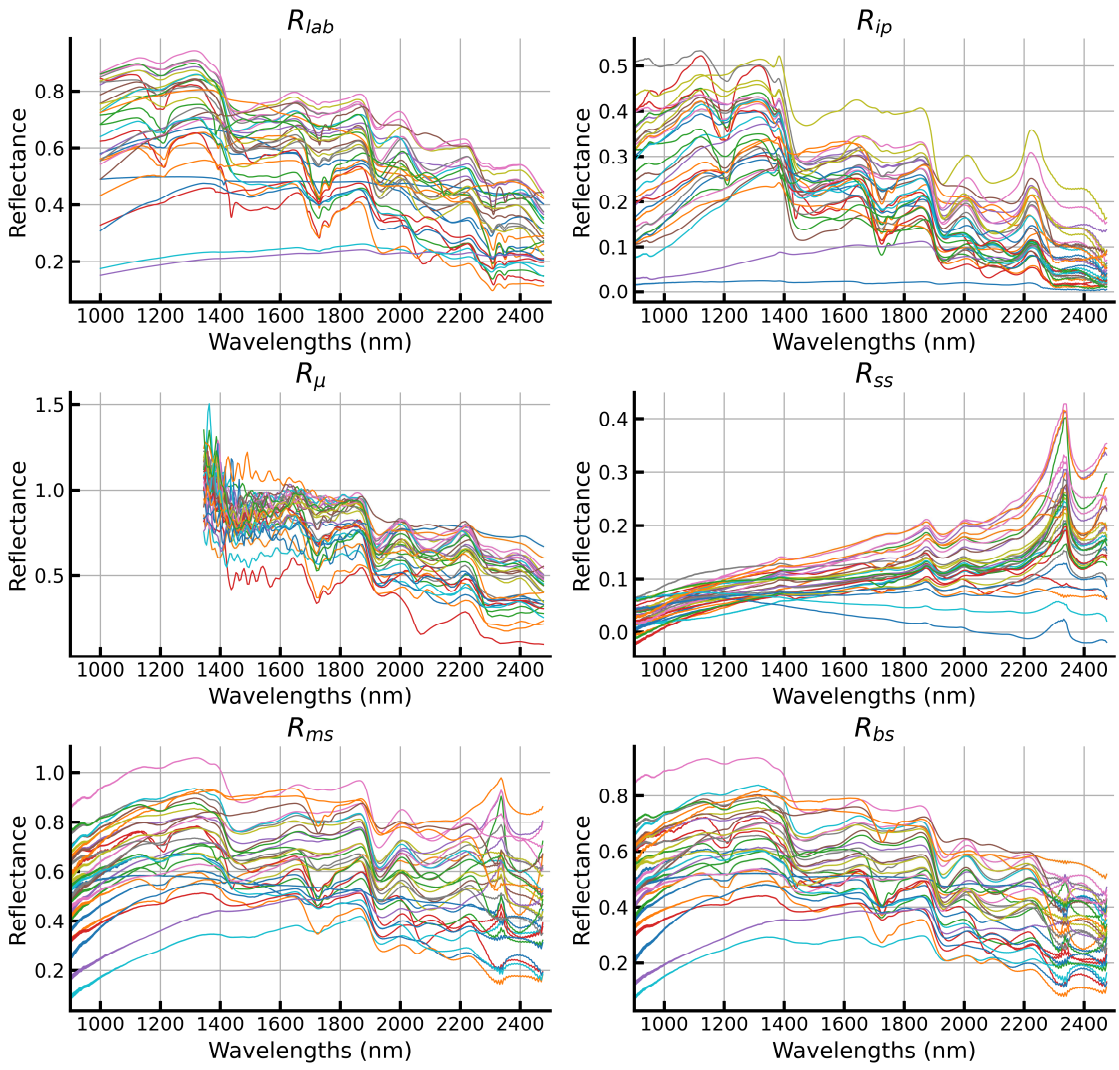

720

721 *Figure 3. Raw reflectance spectra of each spectroscopic system (R_{lab}: laboratory spec-*

722 *trometer, R_{ip}: immersed probe system, R_{μ}: micro-spectrometer, R_{ss}: single scattered signal*

723 *of polarized system, R_{ms}: multiple scattered signal of polarized system, R_{bs}: total back-*

724 *scattered signal of polarized system). Each spectrum corresponds to the mean of the trip-*

725 *licate measurements.*

726

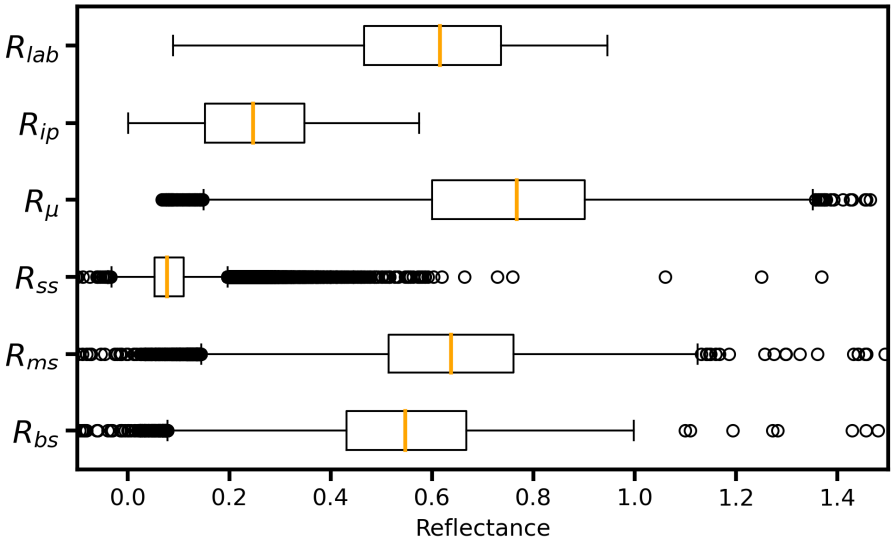

Figure 4. Boxplots of raw reflectance spectra values for each signal type (R_{lab}: laboratory spectrometer, R_{ip}: immersed probe system, R_{μ}: micro-spectrometer, R_{ss}: single scattered signal of polarized system, R_{ms}: multiple scattered signal of polarized system, R_{bs}: total back-scattered signal of polarized system). Each boxplot was obtained on the flattened matrix (reflectance values for all samples and for all wavelengths). Median values are presented with orange lines. The box limits represent the first and third quartile values (respectively $Q1$ and $Q3$), and the lines that extend from the box show the lowest and largest data points excluding any outliers (respectively $Q1 - 1.5 \times (Q3 - Q1)$ and $Q1 - 1.5 \times (Q3 - Q1)$). Outliers are presented in empty black circles.

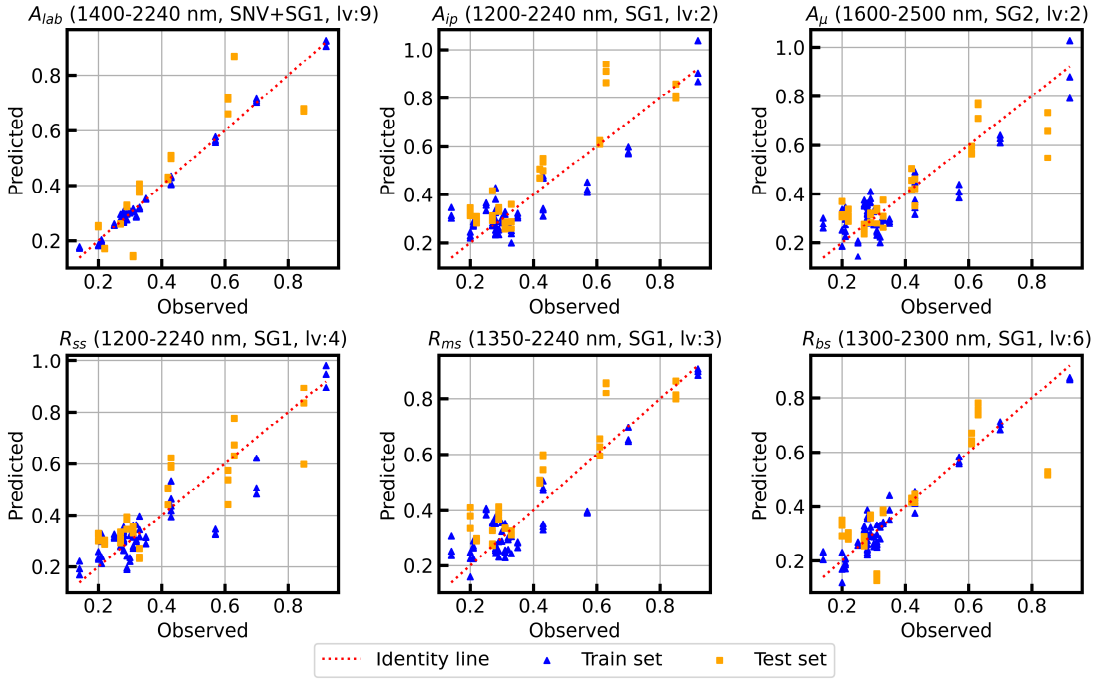

738

739 *Figure 5. Scatter plots of predicted and observed values for the selected prediction models*
740 *of biochemical methane potential (BMP). Each subplot corresponds to the best model se-*
741 *lected for a signal type (from the four spectroscopic configurations). Values for train and*
742 *test sets are respectively presented in blue triangles and orange squares. The spectral*
743 *range, pre-processing type and latent variable number (lv) of the models are provided in*
744 *the titles. Results for other reference characteristics are provided in Appendix D.*

745

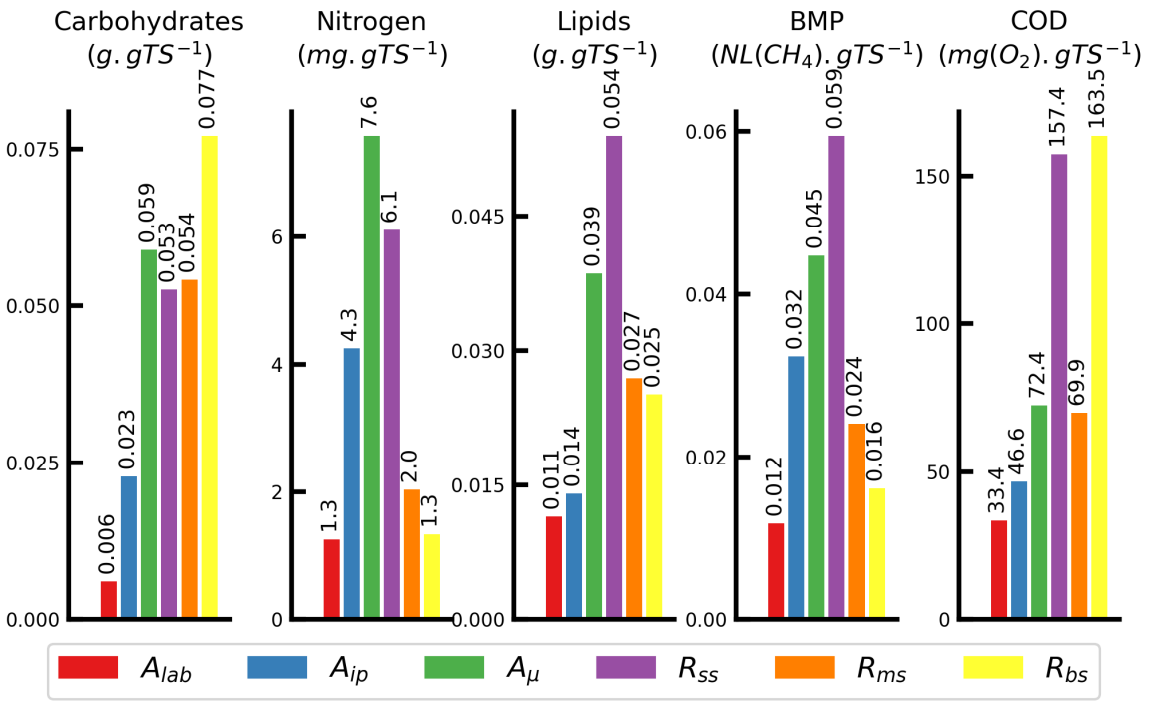

746

747 *Figure 6. Global prediction repeatability standard deviations as calculated with (Eq. 7) and*

748 *(Eq. 8). For each reference characteristic (carbohydrates, nitrogen, lipids, BMP, COD), a*

749 *bar plot colored by signal type is provided (A_{lab} in red, A_{ip} in blue, A_{μ} in green, R_{ss} in violet,*

750 *R_{ms} in orange, and R_{bs} in yellow).*

Graphical abstract

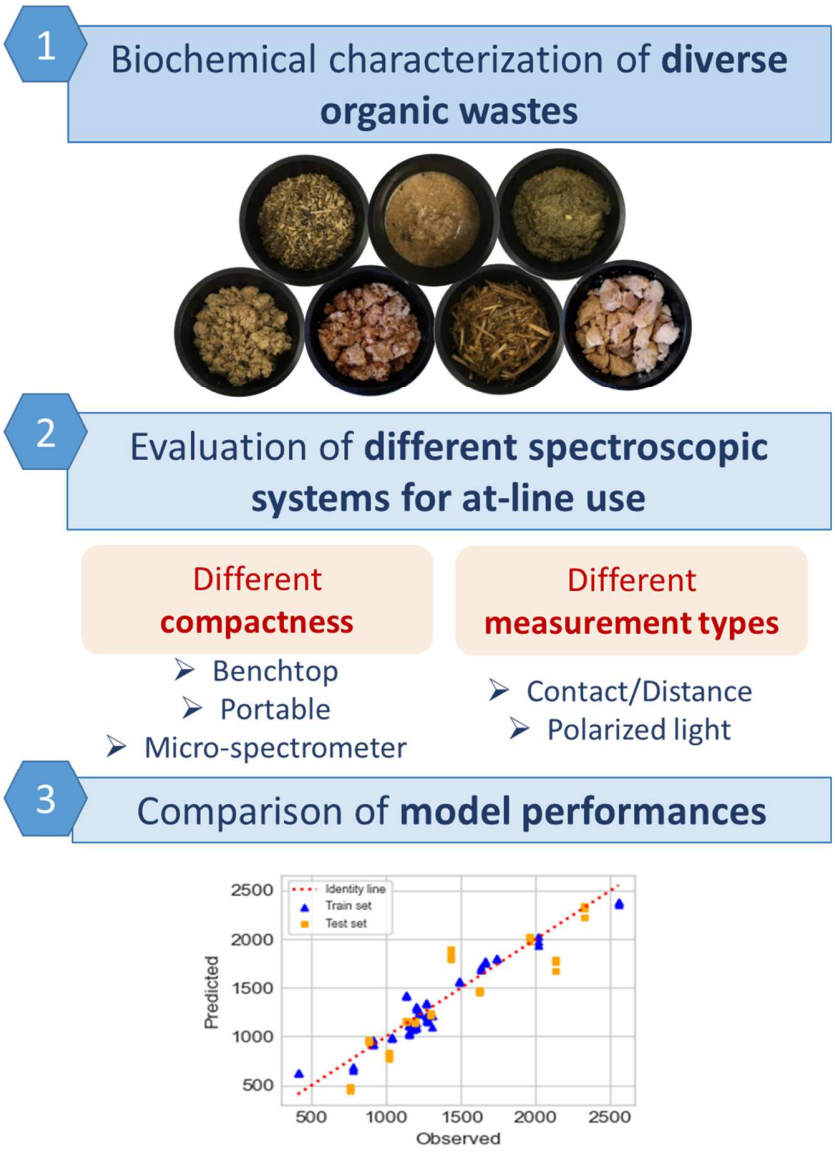

Graphical Abstract - Various organic wastes substrates were collected (1), and spectra were acquired on four different spectroscopic systems (2) with different compactness and measurement types. Then, calibration models were built on each of these spectroscopic systems (3) to predict five different biochemical characteristics (BMP, DCO, Sugar, Nitrogen, Lipids). The spectroscopic systems were compared and evaluated based on the performances of these models.